

---

# Acoustic-Inertial Underwater Navigation

Yulin Yang - yuyang@udel.edu  
Guoquan Huang - ghuang@udel.edu

Department of Mechanical Engineering  
University of Delaware, Delaware, USA

# RPNG

---

Robot Perception and Navigation Group (RPNG)  
Tech Report - RPNG-2016-AINS  
Last Updated - Sept. 29, 2016

# Contents

<b>1</b>	<b>Introduction</b>	<b>1</b>
<b>2</b>	<b>Problem Statement</b>	<b>2</b>
2.1	IMU Kinematic Model . . . . .	2
2.2	Sonar Measurement Model . . . . .	3
2.3	EKF with Stochastic Cloning . . . . .	4
<b>3</b>	<b>Acoustic-Inertial Odometry</b>	<b>5</b>
<b>4</b>	<b>Determining Acoustic Feature Positions</b>	<b>6</b>
4.1	Linear Triangulation . . . . .	6
4.2	Nonlinear Least-Squares . . . . .	8
4.3	Observability Analysis . . . . .	9
<b>5</b>	<b>Simulation Results</b>	<b>9</b>
<b>6</b>	<b>Conclusions and Future Work</b>	<b>14</b>
	<b>Appendix A Proof of Lemma 4.1</b>	<b>15</b>
A.1	Pure rotation around x axis . . . . .	15
A.2	Pure rotation around y axis . . . . .	15
A.3	Pure rotation around z axis . . . . .	16
A.4	Pure translation along x or y axis . . . . .	16
A.5	Pure translation along z axis . . . . .	16
	<b>References</b>	<b>17</b>

## Abstract

In this paper, we introduce a novel acoustic-inertial navigation system (AINS) for Autonomous Underwater Vehicles (AUVs), aiming to reduce the cost and latency of most of current underwater navigation systems that typically employ high-accuracy and thus high-cost inertial sensors. In particular, the proposed approach efficiently fuses the acoustic observations from a 2D imaging sonar and the inertial measurements from a MEMS inertial measurement unit (IMU) within a tightly-coupled EKF framework, while having *no* need to keep the acoustic features in the state vector. As a result, the computational complexity of the proposed AINS is independent of the scale of the operating environment. Moreover, we develop a new acoustic feature linear triangulation to provide accurate initial estimates for iteratively solving the corresponding batch maximum likelihood estimation, and perform an in-depth observability analysis to investigate the effects of sensor motion on the triangulation. Additionally, since it is typically challenging to perform *a priori* sensor extrinsic calibration underwater, we advocate to calibrate IMU-sonar online. The proposed AINS has been validated extensively in Monte-Carlo simulations.

## 1 Introduction

Over the years, there has been increasingly growing demands of Autonomous Underwater Vehicle (AUVs) for a wide range of applications, such as seabed mapping, deep ocean exploring, routine harbor monitoring and oil pipeline maintenance. To successfully accomplish these tasks, an efficient and accurate localization solution is required for AUVs. However, this is challenging for underwater navigation, in part because GPS signal cannot be received underwater, and acoustic beacons require tedious and costly installation before applications. Although high accuracy inertial sensors, such as Doppler Velocity Loggers (DVLs) and fiber optic gyroscopes (FOGs), may provide good localization, the high cost limits their widespread deployments.

Due to the water turbidity and weak illumination in underwater environments, optical cameras only have limited applications and the relatively less expensive two dimensional (2D) forward-looking sonar (FLS) is preferable, which has larger field of view (FOV) and faster operating frequency [1][2], and is often used for short-range underwater detection and imaging [3]. For this reason, substantial research efforts have been taken on sonar-based underwater navigation. Walter et al. [4] used Exactly Sparse Extended Information Filter (ESEIF) with manually extracted sonar features to estimate the trajectory of AUV. Johannsson et al. [5] and Hover et al. [6] both adopted incremental smoothing and mapping (iSAM [7]) to estimate the vehicle motion and produce the environment maps for harbor surveillance and ship hull inspection. In their work automatic feature extraction and Normal Distribution Transformation (NDT) based image registration were introduced. This is different from Hurtos et al. [8], who registered images with Fourier-based methods. Aykin et al. [9] improved [5] by using Gaussian Distribution Transform for image registration instead of NDT. Based on that, Negahdaripour [10] integrated visual cues from acoustic shadows of stationary objects and devised 3D sonar motion estimation solution. Mallios et al. [11] utilized two extended Kalman filters (EKFs) together with a mechanical scanning imaging sonar (MSIS) to solve the full simultaneous localization and mapping (SLAM) problem. Assalih [12] tried a similar idea of stereo vision. Instead of optical cameras, the author imaged with two sonars and estimated the sonar motion by matching corresponding acoustic features between image pairs. Similarly, Negahdaripour et al. [13] proposed an opti-acoustic stereo system, which combined both a DIDSON sonar and an optical camera. But this system is not applicable when there exists strong water turbidity. Based on bundle adjustment (BA) [14], Huang et al. [15] introduced acoustic structure from motion (ASFM), which uses multiple sonar viewpoints to reconstruct 3D structure as well as the motion of sonar.

In contrast to the aforementioned work, in this paper, rather than solely relying on acoustic/optical images, we propose to employ an acoustic sonar and IMU and to develop a low-cost acoustic-inertial navigation system (AINS), by efficiently fusing acoustic measurements from 2D imaging sonar and inertial measurements from a MEMS IMU within a tightly-coupled EKF framework, without keeping the acoustic features in the state vector. In particular, the main theoretical contributions of this work are as follows:

- We develop a novel acoustic-inertial odometry algorithm to fuse acoustic and inertial information without keeping the sonar features in the state vector. Thus, the computational complexity of the proposed approach is independent of the number of features observed.
- We propose a novel acoustic feature triangulation method to provide accurate initial estimates for the iterative algorithms for solving the corresponding batch least-squares problem. Moreover, an in-depth observability analysis is conducted to examine the effects of sensor motion on acoustic feature triangulation.
- We perform online extrinsic calibration between the sonar and the IMU, due to the fact that it is often challenging in practice to pre-calibrate these sensors in operating underwater environments.

The rest of the paper is structured as follows: After formulating the problem in the next section, we present in detail the proposed acoustic-inertial odometry algorithm in Section III. Section IV describes the proposed acoustic feature triangulation as well as the observability analysis. The simulation results of the proposed algorithm are shown in Section V. Finally, we conclude the paper in Section VI as well as possible directions for future research.

## 2 Problem Statement

In this work, we consider a low-cost AUV navigating underwater equipped with a 2D forward looking sonar (FLS) and a MEMS IMU and we aim to efficiently localize the vehicle only using onboard sensor measurements. To this end, in what follows, we briefly describe the IMU kinematic model and the acoustic sonar measurement model within the EKF framework, which will serve as the basis for our proposed AINS.

### 2.1 IMU Kinematic Model

The IMU navigation state  $\mathbf{x}_{IMU}$  is typically given by [16]:

$$\mathbf{x}_{IMU} = [ {}^I_G\bar{q}^T \quad \mathbf{b}_g^T \quad {}^G\mathbf{v}_I^T \quad \mathbf{b}_a^T \quad {}^G\mathbf{p}_I^T ]^T \quad (1)$$

where  ${}^I_G\bar{q}$  is the quaternion representing the rotation from the global frame  $\{G\}$  to the current IMU frame  $\{I\}$  [17].  $b_g$  and  $b_a$  are gyroscope and accelerometer biases for IMU measurements, respectively.  ${}^G\mathbf{v}_I$  and  ${}^G\mathbf{p}_I$  are the IMU velocity and position in the global frame  $\{G\}$ .

The time evolution of the IMU is described as [16, 18]:

$${}^I_G\dot{\bar{q}}(t) = \frac{1}{2}\boldsymbol{\Omega}(\omega_m(t) - \mathbf{b}_g(t) - \mathbf{n}_g(t)){}^I_G\bar{q}(t) \quad (2)$$

$$\dot{\mathbf{b}}_g(t) = \mathbf{n}_{\omega g}(t) \quad (3)$$

$${}^G\dot{\mathbf{v}}_I(t) = \mathbf{R}^T({}^I_G\bar{q})({}^I\mathbf{a}_m - \mathbf{b}_a(t) - \mathbf{n}_a(t)) + {}^G\mathbf{g} \quad (4)$$

$$\dot{\mathbf{b}}_a(t) = \mathbf{n}_{\omega a}(t) \quad (5)$$

$${}^G\dot{\mathbf{p}}_I(t) = {}^G\dot{\mathbf{v}}_I(t) \quad (6)$$

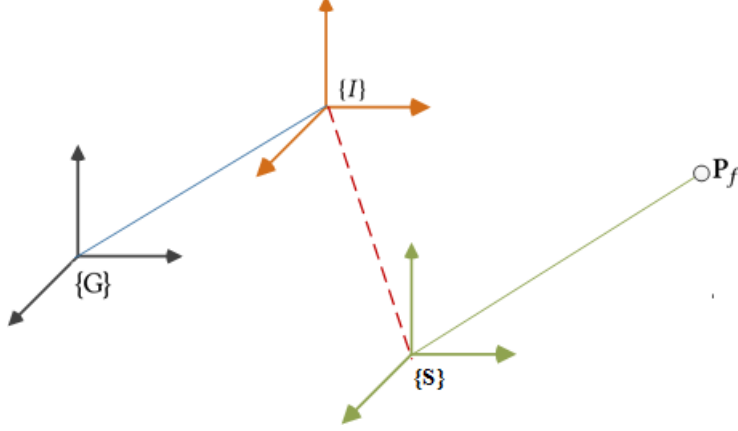


Figure 1: System model introduction:  $\{G\}$  describes the global frame, which the robot motion trajectory will refer to.  $\{I\}$  describes the IMU frame, which the local motion measurements will refer to.  $\{S\}$  is the sonar frames, which the local sonar measurements will refer to. Since IMU is fixed with the sonar sensor, the red dotted line represents the rigid transformation between  $\{I\}$  and  $\{S\}$ .  $\mathbf{P}_f$  denotes the features sensed by sonar.

where  $\mathbf{\Omega}(\omega) = \begin{bmatrix} -[\omega \times] & \omega \\ -\omega^T & 0 \end{bmatrix}$ , and  $\mathbf{R}({}^I_G \bar{q})$  represents the rotation matrix corresponding to  ${}^I_G \bar{q}$ .  $\omega_m$  and  ${}^I \mathbf{a}_m$  are the direct measurements of angular velocity and linear acceleration from IMU, while  $\mathbf{n}_g$  and  $\mathbf{n}_a$  denote the white Gaussian noises that corrupt the corresponding measurements.  $\mathbf{n}_{\omega g}$  and  $\mathbf{n}_{\omega a}$  represents white Gaussian noise vectors driving the IMU biases  $\mathbf{b}_g$  and  $\mathbf{b}_a$ .

## 2.2 Sonar Measurement Model

An imaging sonar (e.g., FLS) provides ranges and azimuth angles to features in the surrounding underwater environment. The acoustic measurement model is depicted in Figure 2. We assume a single feature  $f_j$  has been observed and tracked in a set of  $n$  sonar frames, where the set is denoted as  $M_j$ .

We denote  $f_j$  in the  $i$ -th frame of  $M_j$  as  ${}^{S_i} \mathbf{p}_{f_j}$ , and in the global frame as  ${}^G \mathbf{p}_{f_j}$ , then:

$${}^{S_i} \mathbf{p}_{f_j} = \begin{bmatrix} S_i x_j \\ S_i y_j \\ S_i z_j \end{bmatrix} = \begin{bmatrix} r_{S_i}^{(j)} \cos \phi_{S_i}^{(j)} \cos \theta_{S_i}^{(j)} \\ r_{S_i}^{(j)} \sin \phi_{S_i}^{(j)} \cos \theta_{S_i}^{(j)} \\ r_{S_i}^{(j)} \sin \theta_{S_i}^{(j)} \end{bmatrix} \quad (7)$$

From the sonar measurement, we can get the range  $r_{S_i}^{(j)}$  and the azimuth angle  $\phi_{S_i}^{(j)}$  measurements. Thus, the measurement model can be described as:

$$\mathbf{z}_{S_i}^{(j)} = \begin{bmatrix} r_{S_i}^{(j)} \\ \phi_{S_i}^{(j)} \end{bmatrix} + \mathbf{n}_{S_i}^{(j)} = \begin{bmatrix} \sqrt{S_i x_j^2 + S_i y_j^2 + S_i z_j^2} \\ \arctan \left( \frac{S_i y_j}{S_i x_j} \right) \end{bmatrix} + \mathbf{n}_{S_i}^{(j)} \quad (8)$$

where  $\mathbf{n}_i^{(j)}$  is white Gaussian noise vectors with covariance matrix  $\mathbf{R}_{S_i}^{(j)}$ . We can linearize the measurement model around the state estimate  $\hat{\mathbf{x}}$  and obtain the measurement Jacobian matrix as

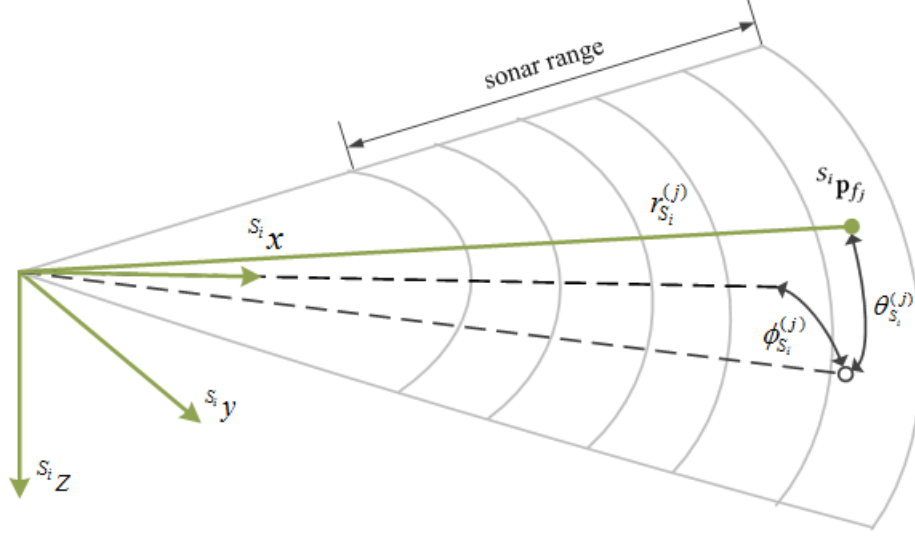


Figure 2: Illustration of the sonar measurement model: The feature  $f_j$  in the sonar frame  $\{S_i\}$ ,  $S_i \mathbf{p}_{f_j}$ , can be represented in a spherical coordinate form:  $(r_i^{(j)}, \phi_i^{(j)}, \theta_i^{(j)})$ . Note that the range  $r_i^{(j)}$  and the azimuth angle  $\phi_i^{(j)}$  of feature  $f_j$  can be derived from this sonar measurement, while the elevation angle  $\theta_i^{(j)}$  is lost in the 2D sonar image.

(which can be used for the EKF update):

$$\frac{\partial \mathbf{z}_{S_i}^{(j)}}{\partial S_i \mathbf{p}_{f_j}} = \begin{bmatrix} \frac{S_i \hat{x}_j}{S_i \hat{r}_j} & \frac{S_i \hat{y}_j}{S_i \hat{r}_j} & \frac{S_i \hat{z}_j}{S_i \hat{r}_j} \\ -\frac{S_i \hat{y}_j}{i \hat{x}_j^2 + S_i \hat{y}_j^2} & \frac{S_i \hat{x}_j}{S_i \hat{x}_j^2 + S_i \hat{y}_j^2} & 0 \end{bmatrix} \quad (9)$$

$$\frac{\partial S_i \mathbf{p}_{f_j}}{\partial S \delta \theta_I} = \left[ \mathbf{R}_I^S(\hat{q}) (\mathbf{R}_G^{I_i}(\hat{q})) ({}^G \hat{\mathbf{p}}_{f_j} - {}^G \hat{\mathbf{p}}_{I_i}) - I \hat{\mathbf{p}}_S \times \right] \quad (10)$$

$$\frac{\partial S_i \mathbf{p}_{f_j}}{\partial I \hat{\mathbf{p}}_S} = -\mathbf{R}_I^S(\hat{q}) \quad (11)$$

$$\frac{\partial S_i \mathbf{p}_{f_j}}{\partial I_i \delta \theta_G} = \mathbf{R}_I^S(\hat{q}) \left[ \mathbf{R}_G^{I_i}(\hat{q}) ({}^G \hat{\mathbf{p}}_{f_j} - {}^G \hat{\mathbf{p}}_{I_i}) \times \right] \quad (12)$$

$$\frac{\partial S_i \mathbf{p}_{f_j}}{\partial G \hat{\mathbf{p}}_{I_i}} = -\mathbf{R}_I^S(\hat{q}) \mathbf{R}_G^{I_i}(\hat{q}) \quad (13)$$

$$\frac{\partial S_i \mathbf{p}_{f_j}}{\partial G \hat{\mathbf{p}}_{f_j}} = \mathbf{R}_I^S(\hat{q}) \mathbf{R}_G^{I_i}(\hat{q}) \quad (14)$$

where  $S_i \hat{r}_j = \sqrt{S_i \hat{x}_j^2 + S_i \hat{y}_j^2 + S_i \hat{z}_j^2}$ .

### 2.3 EKF with Stochastic Cloning

Determining the AUV's poses is often performed using SLAM problem and the EKF (or its variants) is frequently used for solutions (e.g., see [4]). To better address the nonlinear partially-observable sonar measurement [see (8)], we propose to employ stochastic cloning [19] in the EKF framework. Also, we advocate to perform online IMU-Sonar extrinsic calibration, because it is often difficult (if not possible) to pre-calibrate these sensors in an underwater workspace. Specifically, the state

vector at time-step  $k$  contains current IMU state  $\mathbf{x}_{IMU_k}$ , the extrinsic calibration (i.e., 6 DoF rigid transformation) between IMU and sonar  $\mathbf{x}_{calib}$ , the cloned  $N$  latest IMU poses  $\mathbf{x}_{I_i}, i = 1 \dots N$  and all the detected features  $\mathbf{x}_f$ :

$$\mathbf{x}_k = [ \mathbf{x}_{IMU_k}^T \quad \mathbf{x}_{calib}^T \quad \mathbf{x}_{I_1}^T \quad \dots \quad \mathbf{x}_{I_N}^T \quad \mathbf{x}_f^T ]^T \quad (15)$$

where  $\mathbf{x}_{calib} = [ \begin{smallmatrix} S \bar{q}^T & I \mathbf{p}_S^T \end{smallmatrix} ]^T$  is the extrinsic IMU-Sonar calibration;  $\mathbf{x}_{I_i} = [ \begin{smallmatrix} I_i \bar{q}^T & G \mathbf{p}_{I_i}^T \end{smallmatrix} ]^T$  is the  $i$ -th cloned IMU pose, and  $\mathbf{x}_f = [ \begin{smallmatrix} G \mathbf{p}_{f_1}^T & \dots & G \mathbf{p}_{f_{N_L}}^T \end{smallmatrix} ]^T$  contains all  $N_L$  features detected thus far. The standard EKF is then employed to propagate and update the state estimates and covariance [20]. In particular, as a new sonar image is acquired and processed, the current IMU pose estimate ( $I \hat{q}$  and  $G \hat{\mathbf{p}}_I$ ) and newly detected features corresponding to this sonar image will be appended to the state vector and the covariance matrix is augmented accordingly [19]:

$$\mathbf{P}_{k|k} \leftarrow \begin{bmatrix} \mathbf{I}_{6N+21} \\ \mathbf{J} \end{bmatrix} \mathbf{P}_{k|k} \begin{bmatrix} \mathbf{I}_{6N+21} \\ \mathbf{J} \end{bmatrix}^T \quad (16)$$

where the Jacobian  $\mathbf{J}$  is given by (see [19]):

$$\mathbf{J} = \begin{bmatrix} \mathbf{I}_{3 \times 3} & \mathbf{0}_{3 \times 9} & \mathbf{0}_{3 \times 3} & \mathbf{0}_{3 \times (6N+6)} \\ \mathbf{0}_{3 \times 3} & \mathbf{0}_{3 \times 9} & \mathbf{I}_{3 \times 3} & \mathbf{0}_{3 \times (6N+6)} \end{bmatrix}$$

Note that when cloning a new IMU pose, the oldest pose will be removed if the total number of cloned states exceeds the pre-defined threshold.

### 3 Acoustic-Inertial Odometry

It is clear from the preceding section that in the SLAM formulation, as new features are included in the state vector, it may suffer from ever-increasing computational/storage complexity, in particular, when operating in large-scale environments. To address this issue, inspired by visual-inertial odometry [21], we introduce acoustic-inertial odometry for low-cost underwater navigation. In particular, we linearly marginalize out the acoustic features to keep the state vector of constant size, while still utilizing the information of sonar measurements to these features to update state estimates.

Specifically, based on the sonar measurement model (8), the measurement residual for feature  $f_j$  is given by:

$$\mathbf{r}_{S_i}^{(j)} = \mathbf{z}_{S_i}^{(j)} - \hat{\mathbf{z}}_{S_i}^{(j)} \quad (17)$$

Linearizing the above equation around the current state estimates and feature estimates, the measurement residual can be computed as:

$$\mathbf{r}_{S_i}^{(j)} \simeq \mathbf{H}_{\mathbf{x}_{S_i}}^{(j)} \tilde{\mathbf{x}}^* + \mathbf{H}_{f_{S_i}}^{(j)G} \tilde{\mathbf{p}}_{f_j} + \mathbf{n}_{S_i}^{(j)} \quad (18)$$

where  $\mathbf{H}_{\mathbf{x}_{S_i}}^{(j)}$  and  $\mathbf{H}_{f_{S_i}}^{(j)}$  are the Jacobians corresponding to the state vector  $\mathbf{x}^* = [ \mathbf{x}_{IMU_k}^T \quad \mathbf{x}_{calib}^T \quad \mathbf{x}_{I_1}^T \quad \dots \quad \mathbf{x}_{I_N}^T ]^T$  and the sonar feature  $f_j$  respectively. By stacking all the measurement residuals corresponding to the same feature  $f_j$  within the set of  $M_j$ , we have:

$$\mathbf{r}^{(j)} \simeq \mathbf{H}_{\mathbf{x}}^{(j)} \tilde{\mathbf{x}}^* + \mathbf{H}_f^{(j)G} \tilde{\mathbf{p}}_{f_j} + \mathbf{n}^{(j)} \quad (19)$$

where  $\mathbf{H}_{\mathbf{x}}^{(j)}$  and  $\mathbf{H}_f^{(j)}$  are the stacked Jacobians corresponding to state vector and feature  $f_j$  in the set of  $M_j$ . Note that since features are no longer in the state vector, we cannot perform EKF update based on this residual equation (19).

To overcome this issue, similar to [21], we multiply the left nullspace  $\mathbf{U}$  of the Jacobian matrix  $\mathbf{H}_f^{(j)}$  to both sides of (19), and arrive at:

$$\mathbf{r}_o^{(j)} \simeq \mathbf{U}^T \mathbf{H}_{\mathbf{x}}^{(j)} \tilde{\mathbf{x}}^* + \mathbf{U}^T \mathbf{n}^{(j)} \quad (20)$$

$$= \mathbf{H}_o^{(j)} \tilde{\mathbf{x}}^* + \mathbf{n}_o^{(j)} \quad (21)$$

where  $\mathbf{r}_o^{(j)} = \mathbf{U}^T \mathbf{r}^{(j)}$ . Note that here we essentially have linearly marginalized out the features from the linearized measurement model, thus eliminating the need to keep features in the state vector.

With the measurement residual formulation (20) for a single sonar feature, we can stack all the available feature measurements, and thus the stacked residual vector for all features is written as:

$$\mathbf{r} = \mathbf{H} \tilde{\mathbf{x}}^* + \mathbf{n} \quad (22)$$

where  $\mathbf{r}$  and  $\mathbf{n}$  are the stacked residual vectors  $\mathbf{r}_o^{(j)}$  and noise vectors  $\mathbf{n}_o^{(j)}$  respectively, and  $\mathbf{H}$  is the stacked Jacobian matrix of  $\mathbf{H}_o^{(j)}$  corresponding to the state vector. Once we have (22), the standard EKF can be used to update state estimate and covariance [20].

## 4 Determining Acoustic Feature Positions

In order to perform the linear marginalization for the acoustic features as explained in the previous section, the 3D position estimate of the acoustic feature  $f_j$  is needed [see (19)]. Thus, in this section, we present in detail our method of localizing acoustic features.

### 4.1 Linear Triangulation

We first formulate a linear triangulation to obtain the feature position estimates by transforming the nonlinear sonar measurements (8) into linear equations. These triangulation results will be used as the initial estimates for the iterative solver for the nonlinear least-squares (see Section 4.2).

Specifically, let us first consider the bearing constraint. With (7), it is not difficult to see that the bearing of feature  $f_j$  in  $\{S_i\}$  can be written as:

$$\mathbf{b}_{S_i}^{(j)} = \begin{bmatrix} \cos \phi_{S_i}^{(j)} \cos \theta_{S_i}^{(j)} \\ \sin \phi_{S_i}^{(j)} \cos \theta_{S_i}^{(j)} \\ \sin \theta_{S_i}^{(j)} \end{bmatrix} \quad (23)$$

and its perpendicular vector can be computed as:

$$\mathbf{b}_{S_i}^{(j)\perp} = \begin{bmatrix} -\sin \phi_{S_i}^{(j)} & \cos \phi_{S_i}^{(j)} & 0 \end{bmatrix}^T \quad (24)$$

Assuming that  $\{S_N\}$  is the first sonar frame of  $M_j$  and using (23) and (24), we have:

$$\begin{aligned} {}^{S_N} \mathbf{p}_{f_j} &= {}^{S_N} \mathbf{p}_{S_i} + \mathbf{R}^T(S_N \bar{q})^{S_i} \mathbf{p}_{f_j} \Rightarrow \\ \mathbf{R}(S_N \bar{q})^{S_N} {}^{S_N} \mathbf{p}_{f_j} &= \mathbf{b}_{S_i}^{(j)} r_{S_i}^{(j)} + \mathbf{R}(S_N \bar{q})^{S_N} {}^{S_N} \mathbf{p}_{S_i} \Rightarrow \\ (\mathbf{b}_{S_i}^{(j)\perp})^T \mathbf{R}(S_N \bar{q})^{S_N} {}^{S_N} \mathbf{p}_{f_j} &= (\mathbf{b}_{S_i}^{(j)\perp})^T \mathbf{R}(S_N \bar{q})^{S_N} {}^{S_N} \mathbf{p}_{S_i} \end{aligned} \quad (25)$$

where we have employed the identities that  ${}^{S_i}\mathbf{p}_{f_j} = \mathbf{b}_{S_i}^{(j)} r_{S_i}^{(j)}$  and  $(\mathbf{b}_{S_i}^{(j)\perp})^T \mathbf{b}_{S_i}^{(j)} = 0$ .

Now consider the range constraint whose geometry is shown in Figure 3. Based on the law of cosine, we have:

$$\begin{aligned} (r_{S_N}^{(j)})^2 + |{}^{S_N}\mathbf{p}_{S_i}|^2 - (r_{S_i}^{(j)})^2 &= 2r_{S_N}^{(j)} |{}^{S_N}\mathbf{p}_{S_i}| \left( \frac{{}^{S_N}\mathbf{p}_{S_i}}{|{}^{S_N}\mathbf{p}_{S_i}|} \right)^T \mathbf{b}_{S_N}^{(j)} \\ \Rightarrow {}^{S_N}\mathbf{p}_{S_i}^T {}^{S_N}\mathbf{p}_{f_j} &= \frac{1}{2} ((r_{S_N}^{(j)})^2 + |{}^{S_N}\mathbf{p}_{S_i}|^2 - (r_{S_i}^{(j)})^2) \end{aligned} \quad (26)$$

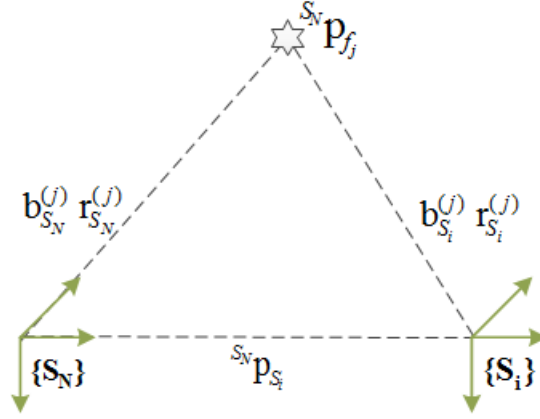


Figure 3: Illustration of the geometry of the acoustic feature triangulation.

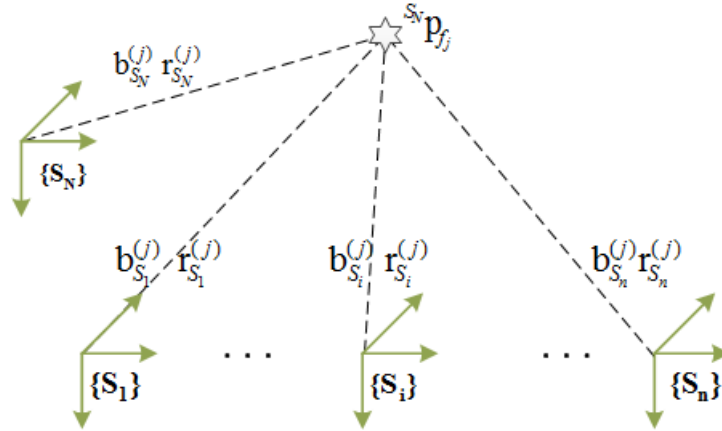


Figure 4: Multiple bearing and range measurements from a sonar to the feature  $f_j$ , which has been observed and tracked in a set of  $n$  sonar frames  $M_j$ . Feature  $f_j$  is first observed in the sonar frame  $\{S_N\}$ , which is also one frame of  $M_j$ .

Since the feature  $f_j$  has been observed and tracked in the set of  $M_j$  frames, which contain  $n$  sonar images, we collect all the measurements from this set and formulate the following linear

least-squares equations:

$$\underbrace{\begin{bmatrix} (\mathbf{b}_{S_1}^{(j)\perp})^T \mathbf{R}_{(S_N \bar{q})}^{(S_1)} \\ S_N \mathbf{p}_{S_1}^T \\ \vdots \\ (\mathbf{b}_{S_i}^{(j)\perp})^T \mathbf{R}_{(S_N \bar{q})}^{(S_i)} \\ S_N \mathbf{p}_{S_i}^T \\ \vdots \\ (\mathbf{b}_{S_n}^{(j)\perp})^T \mathbf{R}_{(S_N \bar{q})}^{(S_n)} \\ S_N \mathbf{p}_{S_n}^T \end{bmatrix}}_{\mathbf{B}_{2n \times 3}} \mathbf{p}_{f_j} = \underbrace{\begin{bmatrix} (\mathbf{b}_{S_1}^{(j)\perp})^T \mathbf{R}_{(S_N \bar{q})}^{(S_1)} S_N \mathbf{p}_{S_1} \\ \frac{1}{2}((r_{S_N}^{(j)})^2 + |S_N \mathbf{p}_{S_1}|^2 - (r_{S_1}^{(j)})^2) \\ \vdots \\ (\mathbf{b}_{S_i}^{(j)\perp})^T \mathbf{R}_{(S_N \bar{q})}^{(S_i)} S_N \mathbf{p}_{S_i} \\ \frac{1}{2}((r_{S_N}^{(j)})^2 + |S_N \mathbf{p}_{S_i}|^2 - (r_{S_i}^{(j)})^2) \\ \vdots \\ (\mathbf{b}_{S_n}^{(j)\perp})^T \mathbf{R}_{(S_N \bar{q})}^{(S_n)} S_N \mathbf{p}_{S_n} \\ \frac{1}{2}((r_{S_N}^{(j)})^2 + |S_N \mathbf{p}_{S_n}|^2 - (r_{S_n}^{(j)})^2) \end{bmatrix}}_{\mathbf{b}_{2n \times 1}} \quad (27)$$

It is clear from (27) that each sonar measurement can provide 2 constraint equations. Therefore, if there are  $n$  ( $n \geq 2$ ) measurements, we are able to determine the feature 3D position in the local sonar frame. Thus, the solution of (27) is given by the normal equation:

$$S_N \mathbf{p}_{f_j} = (\mathbf{B}^T \mathbf{B})^{-1} \mathbf{B}^T \mathbf{b} \quad (28)$$

## 4.2 Nonlinear Least-Squares

Since the above linear triangulation does not take into account the measurement uncertainty, the result would not be optimal in maximum likelihood sense. In order to find the maximum likelihood estimate of the feature, we thus formulate the equivalent (under mild assumptions) nonlinear least-squares optimization to refine the triangulation result:

$$S_i \mathbf{p}_{f_j} = [ S_i x_j \quad S_i y_j \quad S_i z_j ]^T \quad (29)$$

$$= \mathbf{R}_{(S_N \bar{q})}^{(S_i)} \left( \begin{bmatrix} S_N x_j \\ S_N y_j \\ S_N z_j \end{bmatrix} - S_N \mathbf{p}_{S_i} \right) \quad (30)$$

$$= \begin{bmatrix} h_{i1}(S_N x_j, S_N y_j, S_N z_j) \\ h_{i2}(S_N x_j, S_N y_j, S_N z_j) \\ h_{i3}(S_N x_j, S_N y_j, S_N z_j) \end{bmatrix} \quad (31)$$

where  $h_{i1}$ ,  $h_{i2}$ ,  $h_{i3}$  are scalar functions of  $S_N x_j$ ,  $S_N y_j$  and  $S_N z_j$ . Substituting into Eq.(8) we can express the measurement equations as functions containing  $S_N x_j$ ,  $S_N y_j$  and  $S_N z_j$ :

$$\mathbf{z}_{S_i}^{(j)} = h(S_N x_j, S_N y_j, S_N z_j) + \mathbf{n}_{S_i}^{(j)} \quad (32)$$

$$= \begin{bmatrix} \sqrt{h_{i1}^2 + h_{i2}^2 + h_{i3}^2} \\ \arctan\left(\frac{h_{i2}(S_N x_j, S_N y_j, S_N z_j)}{h_{i1}(S_N x_j, S_N y_j, S_N z_j)}\right) \end{bmatrix} + \mathbf{n}_{S_i}^{(j)} \quad (33)$$

We can setup the cost function as following:

$$\min_{S_N \mathbf{p}_{f_j}} \sum_{i=1}^n \left\| \mathbf{z}_{S_i}^{(j)} - h(S_N x_j, S_N y_j, S_N z_j) \right\|_{\mathbf{R}_{S_i}^{(j)}}^2 \quad (34)$$

The Gauss-Newton iterative algorithm can be employed to solve this problem by using the triangulation solution (28) as the initial guess.

### 4.3 Observability Analysis

A close inspection of matrix  $\mathbf{B}$  in (28) reveals that it comprises three components: the bearing perpendicular vector  $\mathbf{b}_{S_i}^{(j)\perp}$ , the sensor rotation  $\mathbf{R}_{(S_N \bar{q})}^{(S_i)}$ , and the sensor translation  ${}^{S_N} \mathbf{p}_{S_i}$ . Therefore, it would be important to examine how the sensor motion impacts the feature triangulation and what are the necessary conditions for feasible feature triangulation. In fact, our rigorous analysis shows the following:

**Lemma 4.1.** *The effects of sensor motion on feature triangulation are summarized in Table 1.*

- *If the sonar rotates solely around  $z$  axis, moves along only  $x$  axis or  $y$  axis, or has any other combined motion pattern of the three basic movements, the sonar feature cannot be triangulated.*
- *Once the sonar motion contains one of the other three basic motion pattern (including  $x$  rotation,  $y$  rotation and  $z$  translation), the sonar feature can be triangulated with at least 2 or 3 measurements.*

Table 1: Effects of Sonar Motion on Feature Triangulation

Sensor Motion	Conditions for Feature Triangulation
pure $x$ rotation	$\phi_{S_i}^{(j)} \neq 0$ for at least 3 measurements
pure $y$ rotation	$\phi_{S_i}^{(j)} \neq 0$ for at least 3 measurements
pure $z$ rotation	Not applicable
pure $x$ translation	Not applicable
pure $y$ translation	Not applicable
pure $z$ translation	$\phi_{S_i}^{(j)} \neq 0$ for at least 2 measurements

*Proof.* See Appendix A. □

## 5 Simulation Results

To validate our proposed AINS algorithm, we perform 50 Monte-Carlo simulations under various conditions. For the results presented in this section, we consider an AUV randomly move in the environments where point features are also randomly populated. Figure 3 shows the vehicle’s trajectory and the feature map. All pertinent parameters of the simulation setup are summarized in Table 2. It should be pointed out that the sensor parameters used in this test are realistic and similar to actual sensors. The performance metrics used are the root mean squared error (RMSE) and the normalized estimation error squared (NEES) [20]. The former quantifies the estimation accuracy while the latter is the standard criterion for estimation consistency.

In particular, Figure 6 (a) and (b) show the average RMSE of Monte-Carlo simulations for the vehicle’s orientation and position. Note that the total distance travelled is about 40 meters, while the average position RMSE is about 1 meter, which indicates that the navigation error of the proposed AINS is about 2.5% of the distance travelled. Figure 7 depicts the average NEES

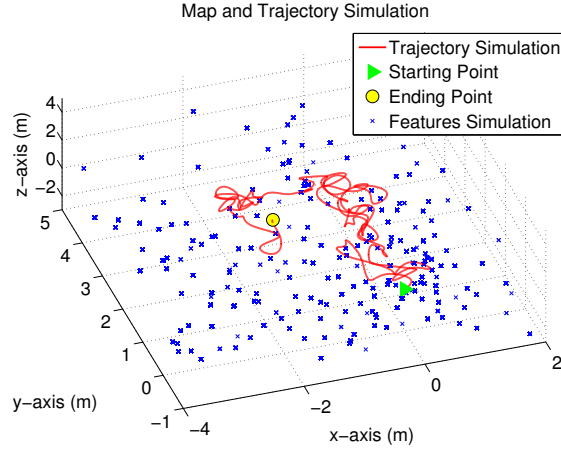


Figure 5: Simulated AUV's trajectory and the feature map.

Table 2: Simulation Setup Parameters

Parameter	Value
Sonar Range (m)	[0.1, 7]
Sonar Azimuth FOV (deg)	[-60,60]
Sonar Elevation FOV (deg)	[-10,10]
Sonar Angular Resolution (deg)	1
Sonar Range Resolution (m)	0.01
Calib Orientation Error (deg)	[3 -3 0]
Calib Orientation $\sigma$ (deg)	4.58
Calib Position Error (m)	[0 0 0.01]
Calib position $\sigma$ (m)	0.2
IMU rotation $\sigma$ (rad/s)	$1.1220 \times 10^{-4}$
IMU rotation bias $\sigma$ (rad/s)	$5.6323 \times 10^{-5}$
IMU acc. $\sigma$ ( $m/s^2$ )	$5.0119 \times 10^{-4}$
IMU acc. bias $\sigma$ ( $m/s^2$ )	$3.9811 \times 10^{-5}$
Monte-Carlo Trials	50

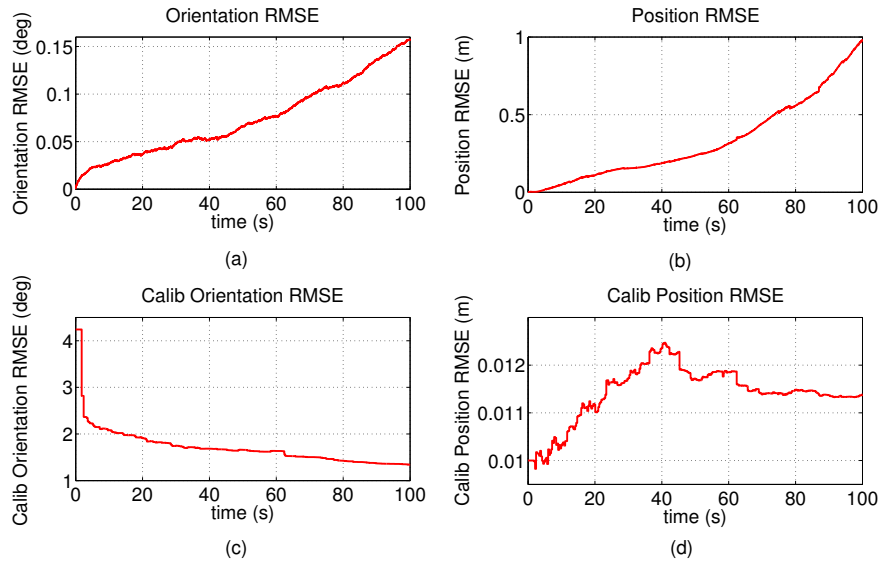


Figure 6: Average RMSE of Monte-Carlo Simulations for the AUV's position and orientation.

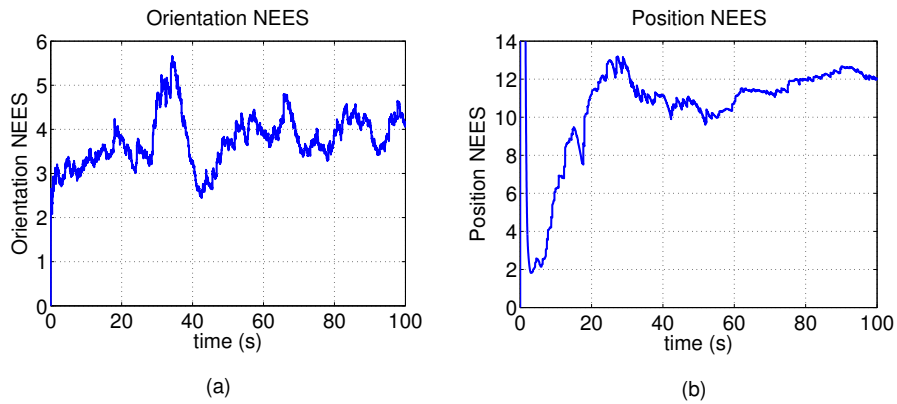


Figure 7: Average NEES of Monte-Carlo Simulations for the AUV's position and orientation.

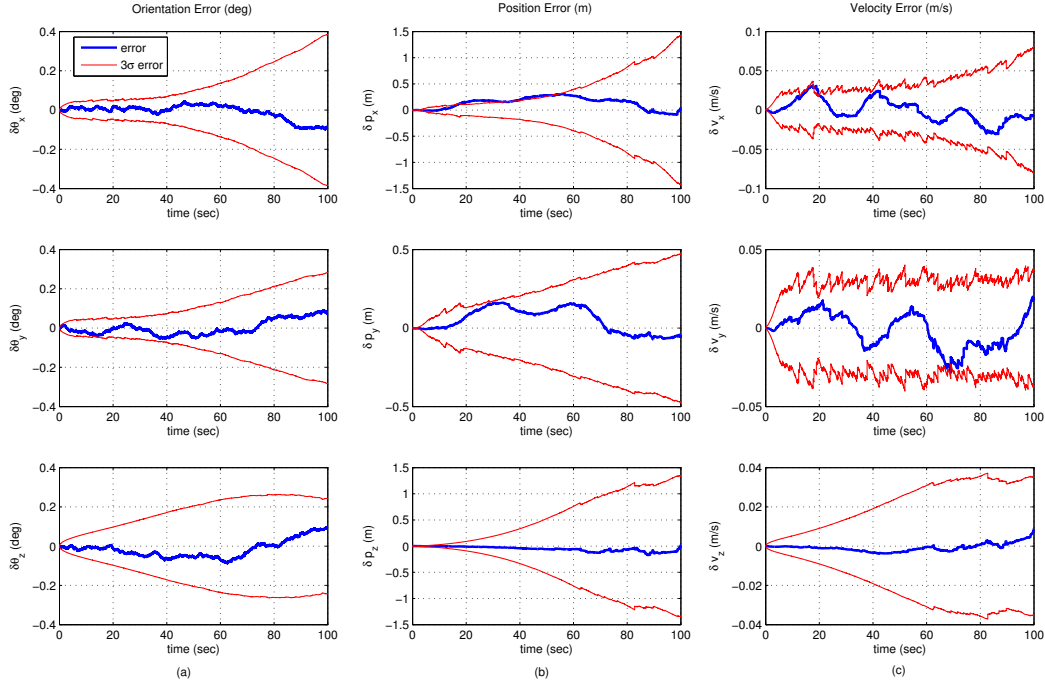


Figure 8: Estimation errors vs.  $3\sigma$  bounds. Note that these results are obtained for one typical realization of the 50 Monte-Carlo simulations.

Table 3: Calib Uncertainty

Calib Orientation(rad)		Calib Position(m)	
Initial $\sigma_\theta$	Stable $\sigma_\theta$	Initial $\sigma$	Stable $\sigma$
$\sigma_{\theta_x} = 0.08$	$\sigma_{\theta_x} = 0.0083$	$\sigma_x = 0.2$	$\sigma_x = 0.0008$
$\sigma_{\theta_y} = 0.08$	$\sigma_{\theta_y} = 0.0102$	$\sigma_y = 0.2$	$\sigma_y = 0.0010$
$\sigma_{\theta_z} = 0.08$	$\sigma_{\theta_z} = 0.0007$	$\sigma_z = 0.2$	$\sigma_z = 0.0063$

of 50 Monte-Carlo simulations for the vehicle’s orientation and position, while Figure 8 shows the estimation errors and the corresponding  $3\sigma$  bounds that are obtained from one typical trial of the 50 Monte Carlo simulations. As evident from these results, the proposed AINS achieves reasonably consistent performance. Figure 6 (c) and (d) show the average RMSE of calibration parameters (rotation and translation). The RMSE for calibration rotation decreases quickly within the first 10 seconds and then stays at a low error value and similarly, the average RMSE for calibration translation converges to a small value. This implies that the online calibration achieves a better accuracy than the initial estimate which is typically obtained by manual measure in practice. Moreover, Figure 9 shows estimate errors and their  $3\sigma$  bounds of the online calibration for a typical trial. Table 3 shows the uncertainty changes for calibration parameters during the representative trial shown in Figure 8. These results show that the online extrinsic calibration for IMU and sonar converges quickly provided good initial estimates and thus in practice, we may stop performing online calibration after a short period of time once its estimate get matured in order to save resources.

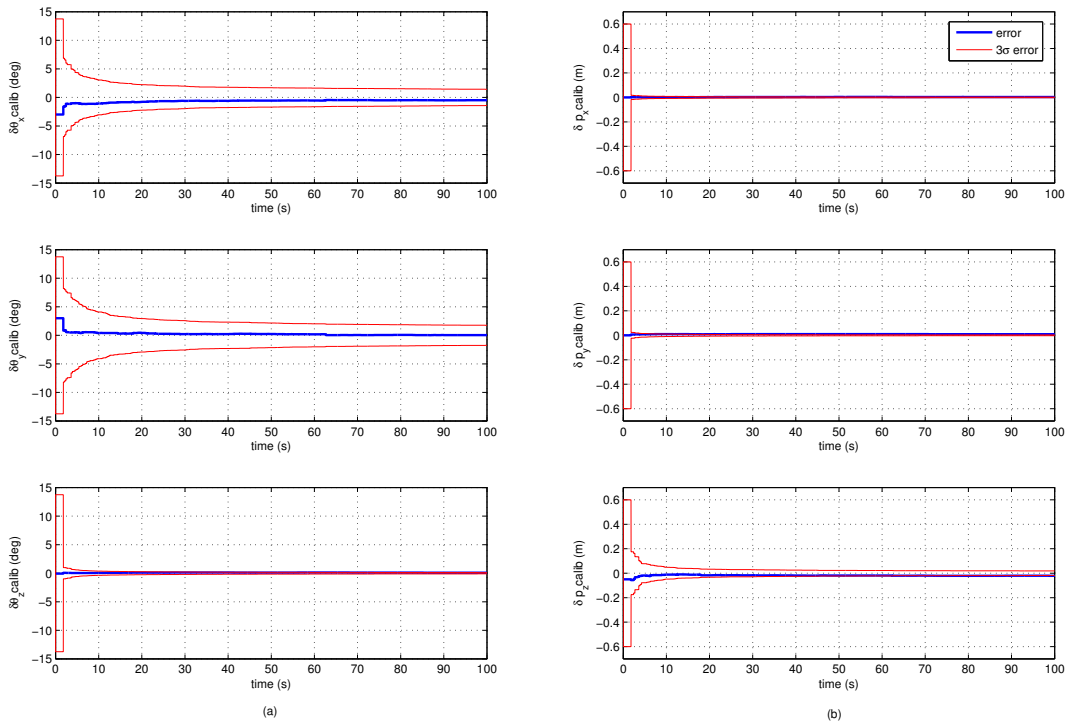


Figure 9: Online calibration errors vs.  $3\sigma$  bounds from one typical run of the 50 Monte-Carlo simulations. (a) and (b) show the  $3\sigma$  bounds and errors of calibration and position respectively in one typical realization of the 50 Monte-Carlo simulations.

## 6 Conclusions and Future Work

We have developed a low-cost acoustic-inertial navigation system (AINS) that efficiently fuses acoustic and inertial measurements within a tightly-coupled, stochastic cloning-based EKF framework. In particular, we linearly marginalize out the acoustic features from the state while still utilizing all the corresponding sonar measurements. As a result, the computational complexity of the proposed approach is independent of the scale of the environment where an AUV operates. We have also introduced a novel acoustic feature linear triangulation to generate initial estimates for the nonlinear least-squares based feature localization. A rigorous, detailed observability analysis has been performed to understand the impact of the sensor motion on the feature triangulation. Additionally, motivated by the practical pre-calibration challenges, the proposed AINS advocates online sonar-IMU extrinsic calibration. Our ongoing work is focusing on validating the proposed AINS algorithm on the real data collected with a Teledyne Gavia [22]. In processing real data, there are two challenging issues that need to be addressed: i) time synchronization between IMU and sonar, and ii) acoustic feature detection and tracking. For time synchronization, we plan to leverage the techniques for IMU-camera synchronization [23] for visual-inertial navigation; and for feature registration, we will investigate the sorting correspondence space (SCS) algorithm that is point-based and proved to be fast and robust in [12].

## Appendix A: Proof of Lemma 4.1

We first introduce the following notations that will be useful for the ensuing analysis:

$${}_{S_N}^{S_i} \mathbf{R} = \begin{bmatrix} r_{11} & r_{12} & r_{13} \\ r_{21} & r_{22} & r_{23} \\ r_{31} & r_{32} & r_{33} \end{bmatrix} \quad (35)$$

$${}^{S_N} \mathbf{p}_{S_i} = [ {}^{S_N} \Delta x_{S_i} \quad {}^{S_N} \Delta y_{S_i} \quad {}^{S_N} \Delta z_{S_i} ]^T \quad (36)$$

$${}^{S_N} \mathbf{p}_{f_j} = [ {}^{S_N} x_j \quad {}^{S_N} y_j \quad {}^{S_N} z_j ]^T \quad (37)$$

### A.1: Pure rotation around x axis

If the sonar only rotates around the  $x$  axis of the local frame, then the rotation matrix  ${}_{S_N}^{S_i} \mathbf{R}$  and the translation vector  ${}^{S_N} \mathbf{p}_{S_i}$  become:

$${}_{S_N}^{S_i} \mathbf{R} = \begin{bmatrix} 1 & 0 & 0 \\ 0 & r_{22} & r_{23} \\ 0 & r_{32} & r_{33} \end{bmatrix}, {}^{S_N} \mathbf{p}_{S_i} = \begin{bmatrix} {}^{S_N} \Delta x_{S_i} \\ {}^{S_N} \Delta y_{S_i} \\ {}^{S_N} \Delta z_{S_i} \end{bmatrix} = \begin{bmatrix} 0 \\ 0 \\ 0 \end{bmatrix}$$

This yields:

$$(\mathbf{b}_{S_i}^{(j)\perp})^T \mathbf{R}_{(S_N \bar{q})}^{(S_i)} {}^{S_N} \mathbf{p}_{f_j} = \begin{bmatrix} -\sin \phi_{S_i}^{(j)} & r_{22} \cos \phi_{S_i}^{(j)} & r_{23} \cos \phi_{S_i}^{(j)} \end{bmatrix} {}^{S_N} \mathbf{p}_{f_j} \quad (38)$$

Thus, from (27), we have:

$$\mathbf{B} = \begin{bmatrix} \vdots & \vdots & \vdots \\ -\sin \phi_{S_i}^{(j)} & r_{22} \cos \phi_{S_i}^{(j)} & r_{23} \cos \phi_{S_i}^{(j)} \\ 0 & 0 & 0 \\ \vdots & \vdots & \vdots \end{bmatrix} \quad (39)$$

Clearly, in this case, at least 3 measurements of feature  $f_j$  with  $\phi_{S_i}^{(j)} \neq 0$  are needed for the triangulation when the sonar is purely rotating around its  $x$  axis.

### A.2: Pure rotation around y axis

Similarly, if the sonar only rotates around the  $y$  axis, then we have:

$${}_{S_N}^{S_i} \mathbf{R} = \begin{bmatrix} r_{11} & 0 & r_{13} \\ 0 & 1 & 0 \\ r_{31} & 0 & r_{33} \end{bmatrix}, {}^{S_N} \mathbf{p}_{S_i} = \begin{bmatrix} 0 \\ 0 \\ 0 \end{bmatrix}$$

$$\mathbf{B} = \begin{bmatrix} \vdots & \vdots & \vdots \\ -r_{11} \sin \phi_{S_i}^{(j)} & \cos \phi_{S_i}^{(j)} & -r_{13} \sin \phi_{S_i}^{(j)} \\ 0 & 0 & 0 \\ \vdots & \vdots & \vdots \end{bmatrix} \quad (40)$$

In this case at least 3 measurements of feature  $f_j$  with  $\phi_{S_i}^{(j)} \neq 0$  are needed for the triangulation.

### A.3: Pure rotation around z axis

If the sonar only rotates around the  $z$  axis of the local frame, then we have:

$$\begin{aligned} \begin{matrix} S_i \\ S_N \end{matrix} \mathbf{R} &= \begin{bmatrix} r_{11} & r_{12} & 0 \\ r_{21} & r_{22} & 0 \\ 0 & 0 & 1 \end{bmatrix}, \begin{matrix} S_N \end{matrix} \mathbf{p}_{S_i} = \begin{bmatrix} 0 \\ 0 \\ 0 \end{bmatrix} \\ \mathbf{B} &= \begin{bmatrix} \vdots & \vdots & \vdots \\ -r_{11} \sin \phi_{S_i}^{(j)} + r_{21} \cos \phi_{S_i}^{(j)} & -r_{12} \sin \phi_{S_i}^{(j)} + r_{22} \cos \phi_{S_i}^{(j)} & 0 \\ 0 & 0 & 0 \\ \vdots & \vdots & \vdots \end{bmatrix} \end{aligned} \quad (41)$$

In this case, we notice that no matter how many measurements are acquired for feature  $f_j$ ,  $\text{Rank}(\mathbf{B}) \leq 2$ . So  $\mathbf{B}^T \mathbf{B}$  will always be singular and the feature cannot be triangulated.

### A.4: Pure translation along x or y axis

If the sonar only has translations along the  $x$  or  $y$  axis of the local frame, then we have:

$$\begin{aligned} \begin{matrix} S_i \\ S_N \end{matrix} \mathbf{R} &= \begin{bmatrix} 1 & 0 & 0 \\ 0 & 1 & 0 \\ 0 & 0 & 1 \end{bmatrix}, \begin{matrix} S_N \end{matrix} \mathbf{p}_{S_i} = \begin{bmatrix} S_N \Delta x_{S_i} \\ S_N \Delta y_{S_i} \\ 0 \end{bmatrix} \\ \mathbf{B} &= \begin{bmatrix} \vdots & \vdots & \vdots \\ -\sin \phi_{S_i}^{(j)} & \cos \phi_{S_i}^{(j)} & 0 \\ S_N \Delta x_{S_i} & S_N \Delta y_{S_i} & 0 \\ \vdots & \vdots & \vdots \end{bmatrix} \end{aligned} \quad (42)$$

In this case,  $\text{Rank}(\mathbf{B}) \leq 2$ . So the feature cannot be triangulated, no matter how many measurements are acquired.

### A.5: Pure translation along z axis

If the sonar only has translations along the  $z$  axis of the local frame, then we have:

$$\begin{aligned} \begin{matrix} S_i \\ S_N \end{matrix} \mathbf{R} &= \begin{bmatrix} 1 & 0 & 0 \\ 0 & 1 & 0 \\ 0 & 0 & 1 \end{bmatrix}, \begin{matrix} S_N \end{matrix} \mathbf{p}_{S_i} = \begin{bmatrix} 0 \\ 0 \\ S_N \Delta z_{S_i} \end{bmatrix} \\ \mathbf{B} &= \begin{bmatrix} \vdots & \vdots & \vdots \\ -\sin \phi_{S_i}^{(j)} & \cos \phi_{S_i}^{(j)} & 0 \\ 0 & 0 & S_N \Delta z_{S_i} \\ \vdots & \vdots & \vdots \end{bmatrix} \end{aligned} \quad (43)$$

In this case, at least 2 measurements of feature  $f_j$  with  $\phi_{S_i}^{(j)} \neq 0$  are needed for the triangulation.

## References

- [1] Behzad Kamgar-Parsi, Lawrence J Rosenblum, and Edward O Belcher. “Underwater imaging with a moving acoustic lens”. In: *IEEE Transactions on Image Processing* 7.1 (1998), pp. 91–99.
- [2] R. L. Thompson. “Blazed array sonar systems - a new technology for creating low-cost high-resolution imaging sonar system for fisfisher management”. In: *Proc. Puget Sound Georgia Basin Research Conference* (2005).
- [3] Shahriar Negahdaripour. “On 3-D scene interpretation from FS sonar imagery”. In: *2012 Oceans*. IEEE. 2012, pp. 1–9.
- [4] Matthew Walter, Franz Hover, and John Leonard. “SLAM for ship hull inspection using exactly sparse extended information filters”. In: *IEEE International Conference on Robotics and Automation*. IEEE. 2008, pp. 1463–1470.
- [5] Hordur Johannsson et al. “Imaging sonar-aided navigation for autonomous underwater harbor surveillance”. In: *2010 IEEE/RSJ International Conference on Intelligent Robots and Systems (IROS)*. IEEE. 2010, pp. 4396–4403.
- [6] Franz S Hover et al. “Advanced perception, navigation and planning for autonomous in-water ship hull inspection”. In: *The International Journal of Robotics Research* 31.12 (2012), pp. 1445–1464.
- [7] M. Kaess, A. Ranganathan, and F. Dellaert. “iSAM: Incremental Smoothing and Mapping”. In: *IEEE Transactions on Robotics* 24.6 (Dec. 2008), pp. 1365–1378.
- [8] Natalia Hurtós, Yvan Petillot, Joaquim Salvi, et al. “Fourier-based registrations for two-dimensional forward-looking sonar image mosaicing”. In: *2012 IEEE/RSJ International Conference on Intelligent Robots and Systems*. IEEE. 2012, pp. 5298–5305.
- [9] Murat D Aykin and Shahriar Negahdaripour. “On Feature Matching and Image Registration for Two-dimensional Forward-scan Sonar Imaging”. In: *Journal of Field Robotics* 30.4 (2013), pp. 602–623.
- [10] Shahriar Negahdaripour. “On 3-D motion estimation from feature tracks in 2-D fs sonar video”. In: *IEEE Transactions on Robotics* 29.4 (2013), pp. 1016–1030.
- [11] Angelos Mallios et al. “Pose-based SLAM with probabilistic scan matching algorithm using a mechanical scanned imaging sonar”. In: *OCEANS 2009-EUROPE*. IEEE. 2009, pp. 1–6.
- [12] Hassan Assalih. “3D reconstruction and motion estimation using forward looking sonar”. PhD thesis. Heriot-Watt University, 2013.
- [13] Shahriar Negahdaripour, Hicham Sekkati, and Hamed Pirsiavash. “Opti-acoustic stereo imaging: On system calibration and 3-D target reconstruction”. In: *IEEE Transactions on image processing* 18.6 (2009), pp. 1203–1214.
- [14] Bill Triggs et al. “Bundle Adjustment – A Modern Synthesis”. In: *Lecture Notes in Computer Science* 1883 (Jan. 2000), pp. 298–375.
- [15] Tiffany A Huang and Michael Kaess. “Towards acoustic structure from motion for imaging sonar”. In: *2015 IEEE/RSJ International Conference on Intelligent Robots and Systems (IROS)*. IEEE. 2015, pp. 758–765.
- [16] Nikolas Trawny and Stergios I. Roumeliotis. *Indirect Kalman Filter for 3D Attitude Estimation*. Tech. rep. University of Minnesota, Dept. of Comp. Sci. & Eng., Mar. 2005.

- [17] W. G. Breckenridge. *Quaternions Proposed Standard Conventions*. Interoffice Memorandum IOM 343-79-1199. Pasadena, CA: Jet Propulsion Laboratory, 1999.
- [18] Averil B. Chatfield. *Fundamentals of High Accuracy Inertial Navigation*. Reston, VA: American Institute of Aeronautics and Astronautics, Inc., 1997.
- [19] S. I. Roumeliotis and J. W. Burdick. “Stochastic Cloning: A generalized framework for processing relative state measurements”. In: *Proc. of IEEE Conf. on Robotics and Automation*. Washington, DC, 2002, pp. 1788–1795.
- [20] Y. Bar-Shalom, X. R. Li, and T. Kirubarajan. *Estimation with Applications to Tracking and Navigation*. New York: John Wiley and Sons, 2001.
- [21] A. I. Mourikis and S. I. Roumeliotis. “A multi-state constraint Kalman filter for vision-aided inertial navigation”. In: *Proceedings of the IEEE International Conference on Robotics and Automation*. Rome, Italy, 2007, pp. 3565–3572.
- [22] Teledyne. *Teledyne Gavia*. Available: [http://www.teledynegavia.com/product\\_dashboard/auvs](http://www.teledynegavia.com/product_dashboard/auvs).
- [23] Chao Guo et al. “Efficient Visual-Inertial Navigation using a Rolling-Shutter Camera with Inaccurate Timestamps”. In: *Proc. of the Robotics: Science and Systems Conference*. Berkeley, CA, 2014.